ELSEVIER

journal homepage: www.intl.elsevierhealth.com/journals/cmpb

General bounds for electrode mislocation on the EEG inverse problem

L. Beltrachini, N. von Ellenrieder, C.H. Muravchik*

LEICI, Facultad de Ingeniería, Universidad Nacional de La Plata, Calle 1 y 47, B1900TAG La Plata, Buenos Aires, Argentina

ARTICLE INFO

Article history:
Received 21 December 2009
Received in revised form
30 April 2010
Accepted 18 May 2010

Keywords:
Cramér–Rao bound
Electrode mislocation
EEG
Inverse problem

ABSTRACT

We analyze the effect of electrode mislocation on the electroencephalography (EEG) inverse problem using the Cramér–Rao bound (CRB) for single dipolar source parameters. We adopt a realistic head shape model, and solve the forward problem using the Boundary Element Method; the use of the CRB allows us to obtain general results which do not depend on the algorithm used for solving the inverse problem. We consider two possible causes for the electrode mislocation, errors in the measurement of the electrode positions and an imperfect registration between the electrodes and the scalp surfaces. For 120 electrodes placed in the scalp according to the 10–20 standard, and errors on the electrode location with a standard deviation of 5 mm, the lower bound on the standard deviation in the source depth estimation is approximately 1 mm in the worst case. Therefore, we conclude that errors in the electrode location may be tolerated since their effect on the EEG inverse problem are negligible from a practical point of view.

1. Introduction

The electroencephalography (EEG) inverse problem consists in estimating the neural activity of underlying sources given electric potential measurements on a finite number of points on the scalp. There exists many factors that affect the quality of the solution of this problem, as electronic noise [1], spontaneous brain activity [2] or head model errors [3–6]. The source localization problem requires knowing the EEG electrode positions on the scalp. There exist several methods [7–11] that are usually applied in practice to locate the electrodes and minimize their position errors.

Electrode mislocation is produced by the randomness of the method used to determine their position, as well as by the registration used to fit the electrodes to the scalp surface model. This second error source may be unavoidable since the scalp and soft tissues are slightly deformable and there will be no exact fit between the scalp surface built usually from Magnetic Resonance Images (MRI) of the subject laying down and the set of measured electrode positions. We will assume that the scalp surface obtained from MRI is free from errors, as is common practice in EEG.

The influence of electrode location errors in the inverse problem has been studied before; in [11–15] spherical volume conductor models are adopted, while only in [16] a realistically head shape model is considered. Also, most of these works analyze the effect of electrode mislocation for particular inverse problem solvers. We present a general method to analyze the effects on the inverse problem with a realistic head shape model, using on the Cramér–Rao bound (CRB) [17]. This method provides a tight lower bound of the variance of any unbiased estimator of the source parameters, hence, generalizing previous work, because the result becomes independent of the algorithm.

To quantify the effect of electrode mislocation we adopt a random model for the electrode positions. This randomness affects the forward problem solution through a linear approxi-

* *Corresponding author*. Tel.: +54 221 4259306.
E-mail address: lbeltra@gmail.com (L. Beltrachini).
0169-2607/$ – see front matter
doi:10.1016/j.cmpb.2010.05.008

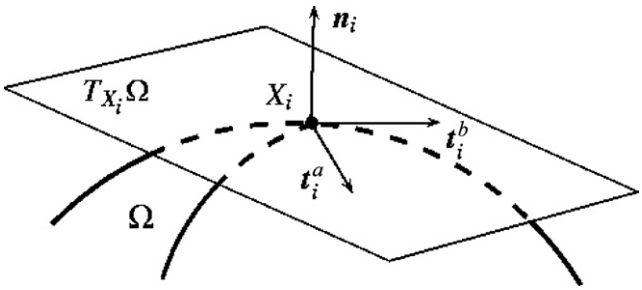

Fig. 1 – Local coordinate system representation for the ith electrode.

mation of the variation of the electric potential around each electrode. Then we compute the sensitivity of the forward problem to the source parameters and obtain the CRB. Our results show that the effect of electrode mislocation is of about the same degree of influence as electronic noise, in agreement with the results of the cited works.

The paper is organized as follows. In Section 2 we introduce the random model adopted to analyze the effects of electrode mislocation. In Section 3 we obtain the Cramér–Rao lower bound for this problem. In Section 4 we discretize the problem using the Boundary Element Method (BEM). In addition we find an expression to evaluate the Cramér–Rao bound numerically, whose results are presented in Section 5. Conclusions and a discussion are presented in Section 6.

2. Random model description

In this section we describe the random model adopted for electrode mislocation. We consider small perturbations of electrodes from their real position that arise from the electrode location technique and the process of fitting the electrodes to the scalp surface image. There are several distinct causes for these errors, and it seems reasonable to consider a Gaussian distribution for the perturbations. Variations in the measured electrode positions with respect to their real positions appear as variations in the electric potential measured in the real position. We find the probability distribution of the electric potential measured, which is used to characterize the influence of electrode mislocation on the inverse problem solution.

Let Ω be the scalp surface where the electrodes are placed on. Let $\mathbb{X}_0 = [X_i^0]_{i=1,\ldots,N_s}$ be the vector whose elements are the actual (unknown) coordinates of the N_s electrodes, and $\mathbb{X} = [X_i]_{i=1,\ldots,N_s}$ their assumed positions, in any coordinate system. For every electrode X_i placed in Ω we define a local coordinate system, given by $\{t_i^a, t_i^b, n_i\}$, where n_i is the unitary vector normal to Ω in X_i and $\{t_i^a, t_i^b\}$ is an orthonormal basis of the plane $T_{X_i}\Omega$ tangent to Ω in X_i (Fig. 1).

If X_i^0 is the real position of the ith electrode, we can say that $X_i = X_i^0 + \xi_i$, where ξ_i is a random variable describing its unknown displacement. If we assume small deviations from X_i^0, we can consider that ξ_i is a vector in $T_{X_i}\Omega$. This can be done due to our assumption of error-less scalp surface image and because electrodes are on the scalp, so the normal component will be neglected since we project the electrode positions to the scalp surface. Errors in the scalp surface model may be considered, but it is not threated in the present work. Then, we can write $\xi_i = \xi_i^a t_i^a + \xi_i^b t_i^b$. We assume that ξ_i^a and ξ_i^b are random Gaussian variables with zero mean, i.e. $E\{X_i\} = X_i^0$. The correlation between the errors in two electrode locations models different error sources. Indeed, the measurement of the electrode positions would have uncorrelated errors for a *one-at-a-time* measurement technique such as digitizers, or a low correlation for other such technique, e.g. [7,10]. On the other hand, the errors due to an imperfect registration between the electrodes and the scalp surface are expected to be highly correlated, since they are related to global quantities such as rotations, translations or scale errors.

Let $\varphi(\chi)$ be the scalar function which denotes the electric potential in some point χ of the scalp surface Ω. Since the solution of the EEG forward problem is continuous in Ω, to be assumed smooth enough with respect to χ, it is possible to write the series expansion of $\varphi(X_i)$ around X_i^0,

$$\varphi(X_i) = \varphi(X_i^0) + \nabla^T \varphi(\chi)\big|_{X_i^0}(X_i - X_i^0) + \cdots \tag{1}$$

Let $\Phi(\mathbb{X}) = [\varphi(X_1), \ldots, \varphi(X_{N_s})]^T$ be the vector of measured potentials, i.e. the electric potential at each of the N_s sensor locations. In this work we consider the average reference montage, i.e. we consider the average of all the measured signals as the reference. Since the potential is a function of the random electrode positions, the vector $\Phi(\mathbb{X})$ is also random. Recalling previous definitions and assumptions, any point X_i can be characterized in the local coordinate system by only two nonzero coordinates, i.e. $X_i = (x_i, y_i, 0)$. Then we can write the electrode positions vector $\mathbb{X}$ as

$$\mathbb{X} = [x_1, \ldots, x_{N_s}, y_1, \ldots, y_{N_s}]^T, \tag{2}$$

and

$$\nabla\Phi(\mathbb{X}_0) = \begin{bmatrix} \left.\frac{\partial\varphi(\chi)}{\partial x_1}\right|_{X_1^0} & \cdots & \left.\frac{\partial\varphi(\chi)}{\partial x_{N_s}}\right|_{X_{N_s}^0} \\ \left.\frac{\partial\varphi(\chi)}{\partial y_1}\right|_{X_1^0} & \cdots & \left.\frac{\partial\varphi(\chi)}{\partial y_{N_s}}\right|_{X_{N_s}^0} \end{bmatrix}^T \tag{3}$$

as the electric potential gradient matrix at the real electrode positions, where each component is in its respective local coordinates system. Therefore, we can write a linear approximation of $\Phi(\mathbb{X})$ around $\mathbb{X}_0$,

$$\Phi(\mathbb{X}) \approx \Phi(\mathbb{X}_0) + ED(\mathbb{X} - \mathbb{X}_0), \tag{4}$$

where $\Phi(\mathbb{X}_0) = [\varphi(X_1^0), \ldots, \varphi(X_{N_s}^0)]^T$, $E = [I_{N_s}|I_{N_s}]$ and $D = diag\{vec(\nabla\Phi(\mathbb{X}_0))\}$. Note that I_N is the $N \times N$ identity matrix, and *diag* and *vec* are the operators that make a diagonal matrix from a vector and vectorize a matrix, respectively.

Under this linear approximation assumption, and since ξ is Gaussian, $\Phi(\mathbb{X})$ will also be a Gaussian random vector whose characterization will be complete with its first and second order moments. The expected value of the potential measurements in (4) is $E\{\Phi(\mathbb{X})\} = \Phi(\mathbb{X}_0)$, the solution of the forward problem for the true electrode positions. The covariance

matrix C_Φ of the electric potential measurements is given by

$$C_\Phi = E\{(\Phi(\mathbb{X}) - E\{\Phi(\mathbb{X})\})(\Phi(\mathbb{X}) - E\{\Phi(\mathbb{X})\})^T\} = E\{ED\mathbb{X}\mathbb{X}^T D^T E^T\} = EDC_{\mathbb{X}} D^T E^T, \quad (5)$$

where $C_{\mathbb{X}} = E\{(\mathbb{X} - \mathbb{X}_0)(\mathbb{X} - \mathbb{X}_0)^T\}$ is the covariance matrix of vector $\mathbb{X}$ and E and D are defined in (4). Thus, $\Phi(\mathbb{X}) \sim \mathcal{N}(\Phi(\mathbb{X}_0), C_\Phi)$, and (5) indicates that the relationship between the measurements covariance matrix C_Φ and the electrode positions covariance $C_{\mathbb{X}}$ depends only on the electric potential gradient.

We consider two different choices for the electrode mislocation spatial covariance matrix $C_{\mathbb{X}}$, to model distinct error sources. We adopt an uncorrelated model, i.e. $C_{\mathbb{X}} = \sigma^2 I_{2N_s}$, to model errors in the measurement of the electrode positions and we adopt a highly correlated jointly Gaussian model with covariance matrix $C_{\mathbb{X}_{ij}} = e^{-(\|X_i - X_j\|_2^2)/2g^2} \mathbf{t}_i^{\alpha_i} \cdot \mathbf{t}_j^{\alpha_j}$, where $g = 10$ cm, and α_k denotes superscript a if $k \le N_s$ or superscript b if $N_s < k \le 2N_s$, to model errors due to a lack of fit between electrodes and scalp surface. In the above formulae, the '·' is the dot product.

3. Performance bounds

The EEG inverse problem consists on estimating source parameters based on noisy electric potential measurements on the scalp. Even though there exist many methods for solving this problem, our goal is to analyze the general influence of uncertainty in the electrode positions on source parameter estimation. This is done with the Cramér–Rao inequality, which gives a lower bound on the variance of estimation errors of any unbiased estimator, regardless of the algorithm used [17]. For multiparameter estimation methods, the Cramér–Rao bound establishes that

$$E\{(\Theta - \hat{\Theta})(\Theta - \hat{\Theta})^T\} \ge CRB(\Theta) = [J(\Theta)]^{-1}, \quad (6)$$

where $\hat{\Theta}$ is any unbiased estimator of the parameter vector Θ, CRB denotes the Cramér–Rao bound, $J(\Theta)$ is the Fisher information matrix and the inequality means that the difference between the matrices is positive definite. For the particular case of normally distributed measurements, the Fisher information matrix is given by [17]

$$J_{ij} = \frac{\partial \Phi(\mathbb{X}_0)^T}{\partial \theta_i} C_\Phi^{-1} \frac{\partial \Phi(\mathbb{X}_0)}{\partial \theta_j} + \frac{1}{2} tr\left\{ C_\Phi^{-1} \frac{\partial C_\Phi}{\partial \theta_i} C_\Phi^{-1} \frac{\partial C_\Phi}{\partial \theta_j} \right\}, \quad (7)$$

where θ_i, $i = 1, \ldots, p$ are the source parameters to be estimated, i.e. elements of Θ. Note that the last term in (7) arises because the covariance matrix C_Φ depends on the source parameters.

If we consider a single static dipolar source [18], we only need to estimate $p = 6$ parameters, three corresponding to source location and the other three corresponding to source strength and orientation. The calculation of (7) will be split into

$$J^0_{ij} = \frac{\partial \Phi(\mathbb{X}_0)^T}{\partial \theta_i} C_\Phi^{-1} \frac{\partial \Phi(\mathbb{X}_0)}{\partial \theta_j}, \quad (8)$$

and

$$J^1_{ij} = \frac{1}{2} tr\left\{ C_\Phi^{-1} \frac{\partial C_\Phi}{\partial \theta_i} C_\Phi^{-1} \frac{\partial C_\Phi}{\partial \theta_j} \right\}. \quad (9)$$

4. Discretization

In this section we use the adopted model to compute the variables required by the bound. The BEM [19,20] is used to discretize the forward problem governing equations, and to compute numerical approximations of the potential, its gradient, and their sensibility to source parameters. With this method the surfaces defining the head model are tessellated in a large number of triangular elements, and a linear system is solved to obtain an approximation to the desired potentials in the vertices of those triangles.

To compute the electric potential we adopt the BEM with linear variation of the potential over the triangular elements [21]. The solution of the forward problem is then given by

$$\Phi(\mathbb{S}) = G\Phi_F, \quad (10)$$

where $\Phi(\mathbb{S})$ is the N elements vector of electric potential at the vertices of the surface tessellated points $\mathbb{S}$, and G is a matrix depending only on the geometry and electric conductivity of the head model. The term Φ_F corresponds to the electric potential generated by the same source of neuronal activity in an homogeneous, infinite media, and can be computed analytically. Since the matrix G does not depend on the source parameters, the sensibility of the electric potential to the source parameters Θ is obtained replacing Φ_F by $\partial\Phi_F/\partial\Theta$ in (10), which we also compute analytically [20]. The corresponding expression is given in Appendix A.

The electric potential at the N_s electrode positions is obtained through linear interpolation of the value on the vertices of the element containing the electrode. Defining the sparse interpolation matrix $H_l(X)$ of size $N_s \times N$, we can write

$$\Phi(\mathbb{X}) = H_l(\mathbb{X})\Phi(\mathbb{S}). \quad (11)$$

Then, we can compute (8) as

$$J^0 = \frac{\partial \Phi(\mathbb{X}_0)^T}{\partial \Theta} C_\Phi^{-1} \frac{\partial \Phi(\mathbb{X}_0)}{\partial \Theta} = \frac{\partial \Phi_F^T}{\partial \Theta} G^T H_l^T(\mathbb{X}_0) C_\Phi^{-1} H_l(\mathbb{X}_0) G \frac{\partial \Phi_F}{\partial \Theta}. \quad (12)$$

To compute the gradient of the electric potential at the electrode positions, we use BEM with the same surface tessellations, but with a constant value for the gradient of the electric potential on each element. The gradient is computed directly, adapting the formulation presented in [22] as explained in Appendix B. This yields

$$vec(\nabla\Phi(\mathbb{S})) = M\mathbf{F}, \quad (13)$$

where the matrix M depends only on the geometry and electric conductivity of the head model. The vector $\mathbf{F}$ is related to the gradient of the electric potential generated by the source in an homogeneous and infinite media; analytic expressions for it and its sensibility to the source parameters are given in

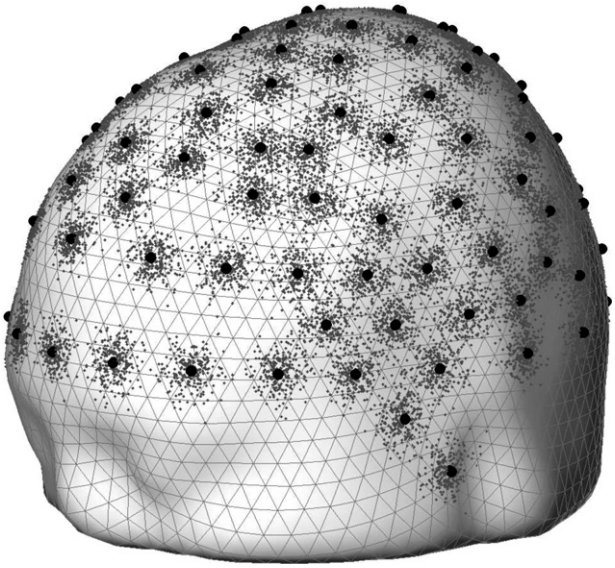

Fig. 2 – Electrode placement adopted over the real head model used. With black dots we denote the mean value of electrode positions, according to an extension of the 10–20 standard. With gray dots we show 250 different realizations of electrode positions, as explained in Section 2. Also, the adopted scalp discretization is shown.

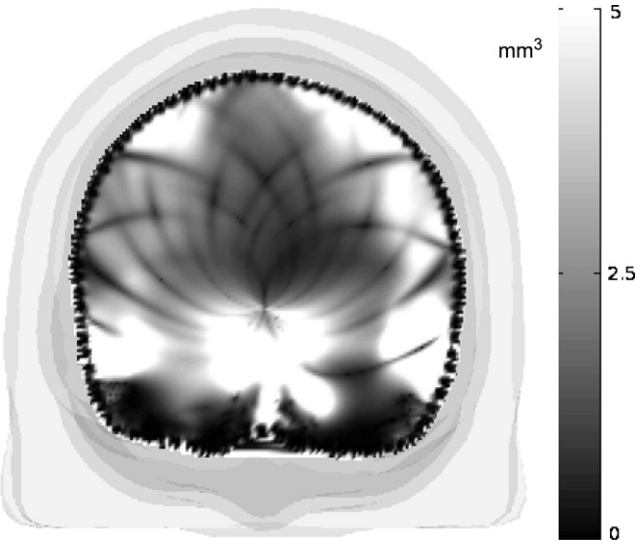

Fig. 3 – Volume of the 90% confidence ellipsoid for source position estimation. Results for a tangentially oriented dipolar source located on a coronal slice of the brain. The gray level indicates the minimum volume of the 90% confidence ellipsoid of any unbiased estimation of the source position.

Appendix A. Again, we use a sparse interpolation matrix $H_F(X)$ to select the element of the scalp tessellation in which each electrode is located. Then, to compute (9), it is easily seen from (5) that

$$\frac{\partial C_\Phi}{\partial \theta_j} = E\left(\frac{\partial D}{\partial \theta_j} C_{\mathbb{X}} D + D C_{\mathbb{X}} \frac{\partial D}{\partial \theta_j}\right) E^T. \tag{14}$$

In the particular case of considering the diagonal covariance matrix (as explained in Section 2), we show in Appendix C that

$$\frac{\partial C_\Phi}{\partial \theta_j} = 2\sigma^2 E\, diag\left\{[(I_2 \otimes H_F^0)M\mathbf{F}] \circ \left[(I_2 \otimes H_F^0)M \frac{\partial \mathbf{F}}{\partial \theta_j}\right]\right\} E^T, \tag{15}$$

where $H_F^0 = H_F(\mathbb{X}_0)$, $\otimes$ denotes the Kronecker product and $\circ$ denotes the element to element or Hadamard matrix multiplication.

5. Numerical results

In this section we use the previous formulation to show the influence of electrode mislocation on the EEG inverse problem solution. We use a realistic head shape model given by a three layered model, with the surfaces between layers tessellated in 2562 vertices (5120 triangular faces), available in the SPM8 software package [23,24]. This discretization gives an average triangle length of approximately 6 mm, which is sufficient to discretize the smooth surfaces considered here. Fig. 2 shows the scalp discretization. The three layers considered correspond to the brain, skull and scalp, with electrical conductivities 0.3 S/m, 0.02 S/m and 0.3 S/m, respectively [25–27]. We used 120 electrodes placed according to an extension of the 10–20 standard [28] (Fig. 2). The forward problem was solved with BEM, as explained in the previous section, with the Isolated Problem Approach [29].

We computed the CRB according to expression (7) and assuming independence between electrode positions. As the CRB for single dipolar sources is a 6×6 matrix that is difficult to visualize, in order to present the results we focus on two quantities related to the source position. The first is the volume of the 90% probability ellipsoid [1,30]. This quantity is a three dimensional confidence interval which quantifies the volume of the ellipsoid that contains the source with 90% probability, considering jointly normal distributions. We also compute the bound of the standard deviation on source depth estimation, which is the square root of the CRB matrix element corresponding to source depth.

In Figs. 3 and 4 we show the volume of the 90% probability ellipsoid and the bound for the standard deviation on depth estimation for tangentially oriented dipoles in a coronal slice view. A point in the slice represents the position of a tangentially oriented dipole and the gray shade is proportional to the volume (Fig. 3) or the standard deviation (Fig. 4). We consider electrode position mislocations with a standard deviation of 5 mm for each electrode. This may be seen as a pessimistic assumption, e.g. the error for manually placed electrodes [16]. The results correspond to a dipolar source of 20 nAm intensity. Note that we have plotted the skin, inskull and outskull meshes only for clarity (the gray level in these layers has no meaning). The figures show that regions with more influence due to electrode mislocation are both the brain cortex (outer layer) and corpus callosum (deepest white matter).

In Fig. 5 we compare the effects on the EEG inverse problem due to electrode mislocation with the effects due to electro-

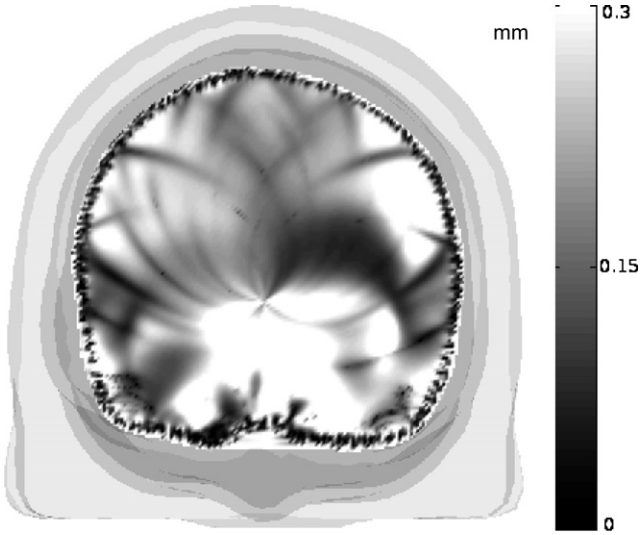

Fig. 4 – Square root of CRB on source depth estimation. Results for a tangentially oriented dipolar source located on a coronal slice of the brain. The gray level indicates the minimum standard deviation for source depth estimation of any unbiased estimation of the source position.

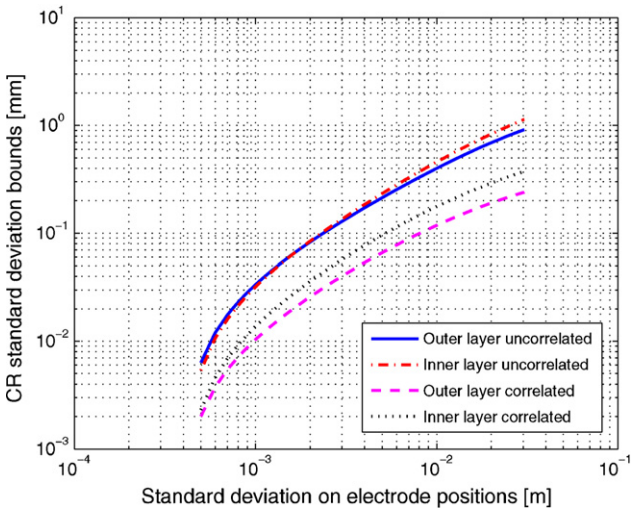

Fig. 6 – Square root of the CRB on source depth estimation versus the standard deviation of electrode positions. Results correspond to the average effects of perturbations on the outer and inner layers considering correlated and uncorrelated electrode positions.

nic noise in sensors. The model we adopted for the electronic noise is Gaussian zero mean and standard deviation 0.5 μV [1], uncorrelated between sensors. Although there exists other error sources, such as correlated background brain activity and modeling errors, we considered the electronic noise because of its unavoidable nature. Fig. 5 shows the ratio between the CRBs on source depth estimation in the presence of electrode mislocation and in the presence of electronic noise as a function of the dipole position. We can see that the influence of electrode position uncertainties is relevant only if we are dealing with sources near the cortex, where its influence is almost equal to the influence of electronic noise in sensors.

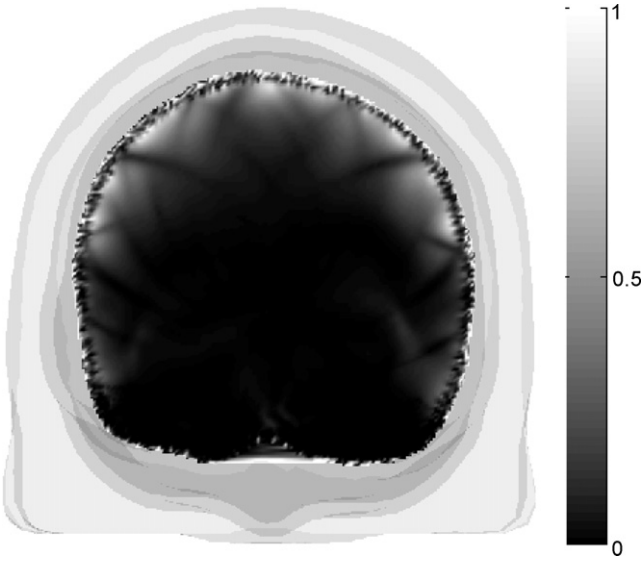

Fig. 5 – Ratio between uncertainties in the inverse problem solution due to the effect on electrode mislocation and due to electronic noise. The ratio is taken between the square root of CRBs on source depth estimation, for each source position.

Some common features may be noted in Figs. 3–5. Dark curved lines crossing the slices can be seen denoting zones where the CRB is lower. They are associated to regions with low magnitude of the electric potential gradient [31]. Also, the results are inaccurate for sources very close to the skull surface, seen in the figures as a thin region with highly varying results. The reason is due to the high numerical errors BEM has for sources with depth less than half the side of the triangular elements of the surface meshes [32].

As mentioned in Section 2, we consider two possible error sources; the electrode mislocation errors modeled as uncorrelated between sensors and the registration error between the electrodes and the scalp surface, modeled as spatially correlated random variables. In Fig. 6 we show a comparison of the results for both cases. The figure shows the lower bound on the standard deviation of unbiased estimators of the source depth, as a function of the standard deviation in the electrode position errors. The sources were separated in two groups, one of them representing dipoles on the gray matter in a layer of 11 mm thickness below the inskull surface, and the inner layer representing dipoles on the white matter. Although it is known that the most important sources of EEG signals are the pyramidal neurons located in gray matter cortex, we simulate sources which could represent deep gray matter in atypical brains. The results shown correspond to the mean value of more than 200 sources in each layer. A comparison of these results and the lower bound on the source depth estimation standard deviation due to typical electronic noise is shown in Fig. 7. It can be seen that the effect of the electrode mislocation is higher for cortical sources and uncorrelated errors in the electrode measurements, but even in the worst case the standard deviation of source depth estimation could be as low as 1 mm, as seen from Fig. 6.

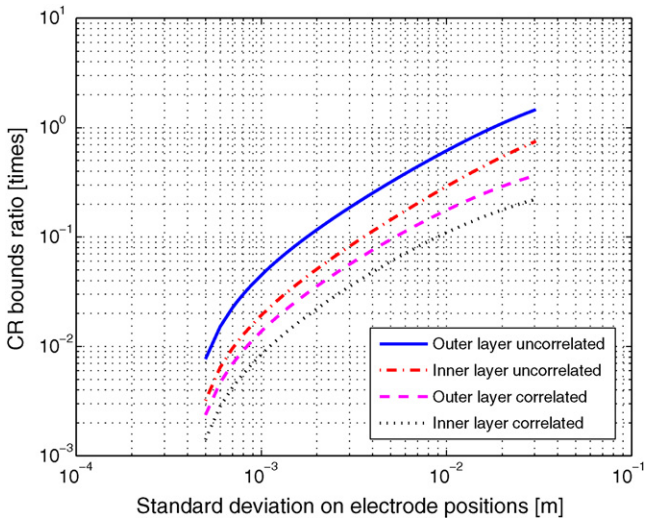

Fig. 7 – Variations on the ratio between the square root of the CRB on depth estimation due to electrode mislocation and due to electronic noise versus the standard deviation of the position of the electrodes. Results correspond to the average effects of perturbations on the outer and inner layers considering correlated and uncorrelated electrode positions.

We show results only for tangentially oriented sources, the effect of electrode mislocation on the inverse problem for sources with radial orientation is computed in the same way. The results are similar, with a slightly smaller effect than for tangentially oriented sources. This seems reasonable since the potential distribution due to radially oriented dipole sources has lower amplitude than the one originated by tangentially oriented dipoles. Also, note that the proposed method can be used to compute the effect of electrode mislocation on parameter estimation of other kinds of sources, i.e. distributed sources, such as line sources [33] or patch sources [34]. This can be accomplished simply by changing the vector $\mathbf{F}$ in Eq. (15). We expect the results to hold for sources that can be modeled as a group of dipoles.

As explained before, we show results considering 120 electrodes on the scalp surface. A similar analysis was made with a 64 electrode configuration, obtaining approximately the same value of the CRB. The ratio between uncertainties in the inverse problem solution due to the efect of eletrode mislocation and due to electronic noise was lower, which was expected since the standard deviation due to the electronic noise grows as the number of electrodes decreases.

6. Conclusions

To quantify the effect of electrode mislocation we model the errors in the electrode positions as random variables, and through a linear approximation of the electric potential around the electrodes determine how this randomness is translated into the forward problem solution. Then, treating this randomness as noise we compute the CRB of the variance of source parameter estimators. The results presented correspond to a general bound on the performance of the estimators, and we do not propose a particular estimator to achieve the stated performance, although some which seem to reach it were proposed in previous works [16,11].

We conclude that the effect of electrode position measurement errors and registration errors between measured electrode positions and the scalp surface are not very important for regular EEG use. In particular, for single dipolar sources we showed that electrode position errors with standard deviation of up to 5 mm lead to negligible estimation errors of the source position when compared to the standard deviation in the estimators due to typical electronic noise of EEG acquisition systems. The largest influence of electrode position errors occurs for tangentially oriented cortical sources. But even in this worst case, the standard deviation bound on the estimation of source position parameters is not larger than 1 mm, and could be neglected when other inaccuracies of the inverse problem are considered, such as spontaneous brain activity [2] or deviations from the adopted three layer homogeneous model [4–6]. Our results also show that the use of an electrode cap, which might introduce correlated errors in the electrode positions, would not imply a lager effect on the inverse problem accuracy than uncorrelated errors of individually placed electrodes.

Finally, we would like to point out that the results are consistent with previous reports for particular inverse problem solvers [16,11], and imply that unavoidable errors from the registration of electrodes and scalp and residual electrode position measurement errors are tolerable in the EEG inverse problem solution. Moreover, the effect of the electrode mislocation is small enough to suggest that a precise electrode position measurement technique is not necessary. However, when all sources of inaccuracy are jointly considered it may still be of practical use for precise studies to know the electrode positions hence, reducing one of these uncertainty causes.

Conflict of interest

None of the authors have any financial or personal relationship with other people or organizations that could inappropriately influence their work.

Acknowledgements

This work was funded by ANPCyT PICT 2007-00535. The work of LB and NvE was supported by CONICET. The work of CHM was supported by CICpBA.

Appendix A.

In this appendix we show expressions for the derivatives $\partial\Phi_F/\partial\Theta$ and $\partial F/\partial\Theta$ mentioned in Section 4. If we consider a single dipolar source placed in $\mathbf{p}$ with dipolar moment $\mathbf{q}$, the parameter vector is the six element vector $\Theta = [\mathbf{p}^T, \mathbf{q}^T]^T$. Let $\mathbf{x}$ be the point of the space where the derivatives are calculated. Here, $\mathbf{x}$ is the set of N points of the inner tesselated surface.

Considering the $N \times 6$ matrix $\partial \Phi_F(\mathbf{x})/\partial \Theta = [\nabla_{\mathbf{p}}^T \Phi_F(\mathbf{x}), \nabla_{\mathbf{q}}^T \Phi_F(\mathbf{x})]^T$ and since $\Phi_F = (1/4\pi r^2)\mathbf{q}\cdot\mathbf{r}$ [20] it is easy to obtain

$$\nabla_{\mathbf{p}} \Phi_F(\mathbf{x}) = \frac{1}{4\pi r^3}(3(\mathbf{q}\cdot\mathbf{r})\mathbf{r} - \mathbf{q}) \tag{A.1}$$

$$\nabla_{\mathbf{q}} \Phi_F(\mathbf{x}) = \frac{1}{4\pi r^2}\mathbf{r}, \tag{A.2}$$

where $r = |\mathbf{x} - \mathbf{p}|$ and $\boldsymbol{r} = (\mathbf{x} - \mathbf{p})/|\mathbf{x} - \mathbf{p}|$.

On the other hand, consider the $2N \times 6$ matrix $\partial \mathbf{F}_i(\mathbf{x})/\partial \Theta = [\nabla_{\mathbf{p}}^T \mathbf{F}_i(\mathbf{x}), \nabla_{\mathbf{q}}^T \mathbf{F}_i(\mathbf{x})]^T$. As seen in Appendix B, there exists a linear dependence between $\mathbf{F}$ and J_{F_i}, where the last one is the only term depending on Θ. In [22] it is shown that

$$J_{F_i} = \frac{1}{4\pi r_i^3}[\mathbf{q} - 3(\mathbf{q}\cdot\mathbf{r}_i)\mathbf{r}_i]. \tag{A.3}$$

Then,

$$\nabla_{\mathbf{p}} \mathbf{F}_i(\mathbf{x}) = \frac{3}{4\pi r_i^4}[\mathbf{r}_i(\mathbf{t}_i^\gamma \cdot \mathbf{q}) - \mathbf{r}_i(\mathbf{q}\cdot\mathbf{r}_i)(\mathbf{t}_i^\gamma \cdot \mathbf{r}_i) + \mathbf{q}(\mathbf{t}_i^\gamma \cdot \mathbf{r}_i) + (\mathbf{q}\cdot\mathbf{r}_i)\mathbf{t}_i^\gamma], \tag{A.4}$$

$$\nabla_{\mathbf{q}} \mathbf{F}_i(\mathbf{x}) = \frac{1}{4\pi r_i^3}[\mathbf{t}_i^\gamma - 3(\mathbf{t}_i^\gamma \cdot \mathbf{r}_i)\mathbf{r}_i], \tag{A.5}$$

where $\gamma = a$ for $i = 1, \ldots, N$ and $\gamma = b$ for $i = N+1, \ldots, 2N$.

Appendix B.

In this appendix we derive the gradient forward problem formulation as stated in Eq. (13). First we find an expression for $\nabla\Phi(\mathbb{S})$. From [22] we know that the gradient of the electric potential in a point S_i of the tessellation $\mathbb{S}$ of Ω is given by

$$\nabla\varphi(S_i) = \frac{1}{\sigma_M}(\mathbf{n}(S_i) \times \mathbf{K}(S_i)), \tag{B.1}$$

where σ_M is the conductivity of the outer layer, $\mathbf{n}(S_i)$ is the unitary vector normal to Ω in S_i and $\mathbf{K}(S_i) = (k_i^a, k_i^b)$ is the equivalent surface current density in the local coordinate system $\{\mathbf{t}_i^a, \mathbf{t}_i^b\}$. It is easily seen that, being $S_i = (w_i, z_i, 0)$ the coordinates in the local coordinate system of S_i, and based on (B.1), the potential gradient in that point is given by

$$\nabla\varphi(S_i) = \begin{bmatrix} \left.\frac{\partial\varphi(\chi)}{\partial w_i}\right|_{S_i} \\ \left.\frac{\partial\varphi(\chi)}{\partial z_i}\right|_{S_i} \end{bmatrix} = \frac{1}{\sigma_M}\begin{bmatrix} -k_i^b \\ k_i^a \end{bmatrix}, \tag{B.2}$$

where the normal component is not included since it is always zero. Replacing (B.2) in $\nabla\Phi(\mathbb{S})$ yields

$$\nabla\Phi(\mathbb{S}) = \frac{1}{\sigma_M}\begin{bmatrix} -k_1^b & \cdots & -k_N^b \\ k_1^a & \cdots & k_N^a \end{bmatrix}^T. \tag{B.3}$$

Based on the original definitions given in [22] we define the matrix G_Δ and the vector $\mathbf{F}$ as

$$G_\Delta = \begin{bmatrix} G_D & -G_C \\ -G_B & G_A \end{bmatrix}, \tag{B.4}$$

$$\mathbf{F} = [\mathbf{t}_1^a \cdot J_{F_1}, \ldots, \mathbf{t}_N^a \cdot J_{F_N}, \mathbf{t}_1^b \cdot J_{F_1}, \ldots, \mathbf{t}_N^b \cdot J_{F_N}]^T, \tag{B.5}$$

where J_{F_i} is the effect of the dipolar source in the local coordinates on the ith element and are the only terms depending on the source parameter. The matrix G_Δ depends only on the model geometry, and is given by

$$\begin{aligned} G_{A_{ij}} &= \mathbf{t}_i^b \cdot (\vec{\Omega}_{ij} \cdot \mathbf{t}_j^a \boldsymbol{n}_j - \Omega_{ij}\mathbf{t}_j^b), \\ G_{B_{ij}} &= \mathbf{t}_i^b \cdot (\vec{\Omega}_{ij} \cdot \mathbf{t}_j^b \boldsymbol{n}_j + \Omega_{ij}\mathbf{t}_j^a), \\ G_{C_{ij}} &= -\mathbf{t}_i^a \cdot (\vec{\Omega}_{ij} \cdot \mathbf{t}_j^a \boldsymbol{n}_j - \Omega_{ij}\mathbf{t}_j^b), \\ G_{D_{ij}} &= -\mathbf{t}_i^a \cdot (\vec{\Omega}_{ij} \cdot \mathbf{t}_j^b \boldsymbol{n}_j + \Omega_{ij}\mathbf{t}_j^a), \end{aligned}$$

where

$$\Omega_{ij} = \frac{1}{4\pi}\int_{\Delta_j} \nabla\left(\frac{1}{r_i}\right)\cdot \boldsymbol{n}_j \, ds_j,$$

$$\vec{\Omega}_{ij} = \frac{1}{4\pi}\int_{\Delta_j} \nabla\left(\frac{1}{r_i}\right)\times \boldsymbol{n}_j \, ds_j,$$

being Δ_j the jth triangle of the surface discretization. We get a linear system whose solution is given by

$$\begin{bmatrix} -\boldsymbol{k}^b \\ \boldsymbol{k}^a \end{bmatrix} = -(\Lambda_K - G_\Delta)^{-1}\mathbf{F} \tag{B.6}$$

where $\boldsymbol{k}^a = [k_1^a, \ldots, k_N^a]^T$ and $\boldsymbol{k}^b = [k_1^b, \ldots, k_N^b]^T$. Replacing (B.6) in (B.3), we find an expression for $vec(\nabla\Phi(\mathbb{S}))$,

$$vec(\nabla\Phi(\mathbb{S})) = M\mathbf{F}, \tag{B.7}$$

where $M = -(1/\sigma_M)(\Lambda_K - G_\Delta)^{-1}$.

Appendix C.

In this appendix we demonstrate (15). As stated in Section 4, the interpolation matrix $H_F(X)$ let us write the potential gradient matrix as

$$\nabla\Phi(\mathbb{X}) = H_F(\mathbb{X})\nabla\Phi(\mathbb{S}). \tag{C.1}$$

Recalling the definition of D given in Section 2 and replacing on it (C.1) yields to

$$D = diag\{vec(\nabla\Phi(\mathbb{X}_0))\} = diag\{vec(H_F(\mathbb{X}_0)\nabla\Phi(\mathbb{S}))\}. \tag{C.2}$$

Using that $vec(AB) = (I_p \otimes A)\,vec(B)$ for $A_{m\times n}$ and $B_{n\times p}$, and (B.7), in (C.2) we get

$$D = diag\{(I_2 \otimes H_F(\mathbb{X}_0))vec(\nabla\Phi(\mathbb{S}))\} = diag\{(I_2 \otimes H_F(\mathbb{X}_0))M\mathbf{F}\}. \tag{C.3}$$

We see that the only factor of D depending on the source parameter vector Θ is $\mathbf{F}$. Therefore, its derivative becomes

$$\frac{\partial D}{\partial \theta_j} = diag\left\{(I_2 \otimes H_F(\mathbb{X}_0))M\frac{\partial \mathbf{F}}{\partial \theta_j}\right\}. \tag{C.4}$$

Next, we want to find an expression for J^1. Using the chain rule and knowing that the only term of C_Φ depending on the source is D, we get

$$\frac{\partial C_\Phi}{\partial \theta_j} = E\frac{\partial (DC_{\mathbb{X}}D)}{\partial \theta_j}E^T = E\left(\frac{\partial D}{\partial \theta_j}C_{\mathbb{X}}D + DC_{\mathbb{X}}\frac{\partial D}{\partial \theta_j}\right)E^T, \tag{C.5}$$

where we use the fact that D is diagonal. If we assume independence between sensor positions, from Section 2 we have $C_{\mathbb{X}} = \sigma^2 I_{2N_s}$. Replacing Eqs. (C.3) and (C.4) in (C.5) we get

$$\begin{aligned}\frac{\partial C_\Phi}{\partial \theta_j} &= 2\sigma^2 E\, diag\{vec(\nabla\Phi(\mathbb{X}_0))\}diag\left\{vec\left(\frac{\partial \nabla\Phi(\mathbb{X}_0)}{\partial \theta_j}\right)\right\}E^T \\ &= 2\sigma^2 E\, diag\left\{vec(\nabla\Phi(\mathbb{X}_0)) \circ vec\left(\frac{\partial \nabla\Phi(\mathbb{X}_0)}{\partial \theta_j}\right)\right\}E^T \\ &= 2\sigma^2 E\, diag\left\{[(I_2 \otimes H_F^0)M\mathbf{F}] \circ \left[(I_2 \otimes H_F^0)M\frac{\partial \mathbf{F}}{\partial \theta_j}\right]\right\}E^T, \end{aligned} \tag{C.6}$$

where $H_F^0 = H_F(\mathbb{X}_0)$.

REFERENCES

[1] C. Muravchik, A. Nehorai, EEG/MEG error bounds for a static dipole source with a realistic head model, IEEE Trans. Signal Process. 49 (3) (2001) 470–484.

[2] H. Huizenga, J. de Munck, L. Waldorp, R. Grasman, Spatiotemporal EEG/MEG source analysis based on a parametric noise covariance model, IEEE Trans. Biomed. Eng. 49 (6) (2002) 533–539.

[3] N. von Ellenrieder, C. Muravchik, A. Nehorai, Effects of geometric head model perturbations on the EEG inverse problem, IEEE Trans. Biomed. Eng. 53 (2) (2006) 249–257.

[4] J. Ollikainen, M. Vauhkonen, P.A. Karjalainen, J.P. Kaipio, Effects of local skull inhomogeneities on EEG source estimation, Med. Eng. Phys. 21 (1999) 143–154.

[5] K. Wendel, N.G. Narra, M. Hannula, P. Kauppinen, J. Malmivuo, The influence of CSF on EEG sensitivity distributions of multilayered head models, IEEE Trans. Biomed. Eng. 55 (4) (2008) 1454–1456.

[6] C.H. Wolters, A. Anwander, D. Weinstein, M. Koch, X. Tricoche, R.S. MacLeod, Influence of tissue conductivity anisotropy on EEG/MEG field and return current computation in a realistic head model: a simulation and visualization study using high-resolution finite element modeling, NeuroImage 30 (3) (2006) 813–826.

[7] J. de Munck, P. Vijn, H. Spekreijse, A practical method for determining electrode positions on the head, Electroencephalogr. Clin. Neurophysiol. 78 (1) (1991) 85–87.

[8] M. Wang, C. Maurer, J. Fitzpatrick, R. Maciunas, An automatic technique for finding and localizing externally attached markers in CT and MR volume images of the head, IEEE Trans. Biomed. Eng. 43 (6) (1996) 627–637.

[9] S. Yoo, C.R. Guttmann, J. Ives, L. Panych, R. Kikinis, D. Schomer, F. Jolesz, 3D localization of surface 10–20 EEG electrodes on high resolution anatomical MR images, Electroencephalogr. Clin. Neurophisiol. 102 (1997) 335–339.

[10] N. von Ellenrieder, L. Beltrachini, A. Blenkmann, J.S. Martín, S. Kochen, C. Muravchik, Determinación de la ubicación de electrodos de EEG basada en fotografías digitales, in: XIII Reunión de Trabajo en Procesamiento de la Información y Control (RPIC 2009), Rosario, Argentina, 2009, pp. 867–880.

[11] D. Khosla, M. Don, B. Kwong, Spatial mislocation of EEG electrodes—effects on accuracy of dipole estimation, Clin. Neurophysiol. 110 (2) (1999) 261–271.

[12] R. Kavanagh, T. Darcey, D. Lehmann, D. Fender, Evaluation of methods for three-dimensional localization of electrical sources in the human brain, IEEE Trans. Biomed. Eng. 25 (5) (1978) 421–429.

[13] V. Towle, J. Bolaños, D. Suarez, K. Tan, R. Grzeszczuk, D. Levin, R. Cakmur, S. Frank, J. Spire, The spatial location of EEG electrodes: locating the best-fitting sphere relative to cortical anatomy, Electroencephalogr. Clin. Neurophysiol. 86 (1993) 1–6.

[14] G.V. Hoey, B. Vanrumste, M. D'Havé, R.V. de Walle, I. Lemahieu, P. Boon, Influence of measurement noise and electrode mislocalisation on EEG dipole-source localisation, Med. Biol. Eng. Comput. 38 (3) (2000) 287–296.

[15] P. Bruno, F. Vatta, P. Inchingolo, Influence of EEG measurement montage on source localization error bounds due to head modeling errors caused by brain lesions, in: Proceedings of the 26th Annual International Conference of the IEEE EMBS, San Francisco, CA, USA, 2004, pp. 825–828.

[16] M. Wang, J. Gotman, The influence of electrode location errors on EEG dipole source localization with a realistic head model, Clin. Neurophysiol. 112 (2001) 1777–1780.

[17] S.M. Kay, Fundamentals of Statistical Signal Processing: Estimation Theory, Signal Processing Series, Prentice-Hall, 1993.

[18] J. de Munck, B.V. Dijk, H. Spekreijse, Mathematical dipoles are adequate to describe realistic generators of human brain activity, IEEE Trans. Biomed. Eng. 35 (1988) 960–966.

[19] D. Geselowitz, On bioelectric potentials in an inhomogenous volume conductor, Biophys. J. 7 (1967) 1–11.

[20] J. Sarvas, Basic mathematical and electromagnetic concepts of the biomagnetic inverse problem, Phys. Med. Biol. 32 (1987) 11–22.

[21] J. de Munck, A linear discretization of the volume conductor boundary integral equation using analytically integrated elements, IEEE Trans. Biomed. Eng. 39 (9) (1992) 986–990.

[22] N. von Ellenrieder, C. Muravchik, A. Nehorai, MEG forward problem formulation using equivalent surface current densities, IEEE Trans. Biomed. Eng. 52 (7) (2005) 1210–1217.

[23] W.T.C. for Neuroimaging Statistic parametrical mapping (SPM) toolbox, http://www.fil.ion.ucl.ac.uk/spm/, 2009.

[24] K.J. Friston, J. Ashburner, S.J. Kiebel, T.E. Nichols, W.D. Penny (Eds.), Statistical Parametric Mapping: The Analysis of Functional Brain Images, Academic Press, 2007.

[25] T. Oostendorp, J. Delbecke, D. Stegeman, The conductivity of the human skull: results of in vivo and in vitro measurements, IEEE Trans. Biomed. Eng. 47 (11) (2000) 1467–1492.

[26] K. Wendel, J. Malmivuo, Correlation between live and post mortem skull conductivity measurements, in: Proceedings of the 28th IEEE EMBS Annual International Conference, New York, USA, 2006.

[27] Y. Zhang, W. van Drongelen, B. He, Estimation of in vivo brain-to-skull conductivity ratio in humans, Appl. Phys. Lett. 89 (4) (2006) 223903–2239033.

[28] G. Deuschl, A. Eisen, Recommendations for the practice of clinical neurophysiology: guidelines of the International Federation of Clinical Neurophysiology, 2nd edition, Electroencephalogr. Clin. Neurophysiol. (Suppl. 52), Elsevier Science B.V., 1999.

[29] J. Meijs, O. Weier, M. Peters, A. van Oosterom, On the numerical accuracy of the boundary element method, IEEE Trans. Biomed. Eng. 36 (1989) 1038–1049.
[30] B. Hochwald, A. Nehorai, Magnetoencephalography with diversely oriented and multi component sensors, IEEE Trans. Biomed. Eng. 44 (1997) 40–50.
[31] N. von Ellenrieder, C. Muravchik, Comparación entre sensores de potencial y gradiente de potencial en mediciones de EEG, in: Actas del XVII Congreso Argentino de Control Automático (AADECA 2000), Buenos Aires, Argentina, 2000, pp. 389–394.
[32] J. Haueisen, A. Büttner, M. Funke, H. Brauer, H. Nowak, Influence of boundary element discretization on the forward and inverse problem in electroencephalography and magnetoencephalography, Biomed. Tech. 42 (1997) 240–248.
[33] I. Yetik, A. Nehorai, C. Muravchik, J. Haueisen, Line source modeling and estimation with magnetoencephalography, in: IEEE International Symposium on Biomedical Imaging: Nano to Macro, vol. 2, 2004, pp. 1339–1342.
[34] I. Yetik, A. Nehorai, C. Muravchik, J. Haueisen, M. Eiselt, Surface-source modeling and estimation using biomagnetic measurements, IEEE Trans. Biomed. Eng. 53 (10) (2006) 1872–1882.